Robotica (2014) volume 32, pp. 1005–1015. © Cambridge University Press 2014
doi:10.1017/S0263574713001215

Modeling of contact pressure distribution and friction limit surfaces for soft fingers in robotic grasping

Sadeq Hussein Bakhy*

Department of Machines and Equipment Engineering, University of Technology, Baghdad, Iraq

(Accepted November 26, 2013. First published online: January 2, 2014)

SUMMARY

A new theory in contact pressure distribution and friction limit surfaces for modeling of hemicylindrical soft fingertips is introduced, to define the relationship between friction force and the moment with respect to the normal axis of contact. A general pressure-distribution function is proposed to capture material properties and contact geometry with various pressure profiles, and the coefficient of pressure distribution over the rectangular contact area is found between π and $\pi/2$. Combining the results of the contact mechanics model with the contact pressure distribution, the normalized friction limit surface can be derived for anthropomorphic soft fingers. The numerical friction limit surface of hemicylindrical soft-finger contact can be approximated by an ellipse, with the major and minor axes as the maximum friction force and the maximum moment with respect to the normal axis of contact, respectively. The results show that the friction limit surfaces are improved (13%–17%), if hemicylindrical fingertips are used rather than hemispherical fingertips at the same radius of fingertip, shape factor of the pressure profile, and applied load. Furthermore, the results of the contact mechanics model and the pressure distribution for soft fingers facilitate the construction of numerical friction limit surfaces, enabling to analyze and simulate the contact behaviors of grasping and manipulation in humanoid robots, prosthetic hands, and robotic hands.

KEYWORDS: Humanoid robots; Grasping; Robotic hands; Novel applications of robotics; Nonprehensile manipulation.

List of symbols

Symbols	Definition	Units
A	Contact area	mm^2
a	Half width contact of rectangular contact area for hemicylindrical fingertips	mm
B	Aspect ratio of rectangular contact	–
c_{cy}	Constant that depends on the size, depth, and curvature of the hemicylindrical fingertip	–
C_k	The coefficient of pressure distribution over the contact area	–
d_c	Displacement of the center of rotation (COR) along the X-axis	mm
dA	Infinitesimal contact area	mm^2
f_x, f_y	Tangential force along the X-axis and Y-axis, respectively	N
f_t	Total tangential force over the entire contact area	N
k	Shape factor of the pressure profile	–
l	Half depth contact of rectangular contact area	mm
L	Depth contact of rectangular contact area (i.e., $L = 2l$)	mm
m_z	The moment about the Z-axis	N·mm
n	Stress exponent for nonlinear elastic materials (strain-hardening factor)	–

* Corresponding author. E-mail: sadeqbakhy@yahoo.com

N	The normal force	N
P	Pressure distribution	Pa
$\boldsymbol{u}$	Velocity vector	mm/s
x	The distance from the center of rectangular contact area with $0 \leq x \leq l$	mm
y	The distance from the center of rectangular contact area with $0 \leq \mathrm{y} \leq a$	mm
X, Y, Z	Citizen coordinates	–
$\boldsymbol{w}$	Total wrench vector the part applies to the support	N·mm
$\tilde{\lambda}$	The normalized characteristic pitches	–
υ	Linear velocity vector	mm/s
$\tilde{\boldsymbol{\upsilon}}$	Unit velocity	–
μ	The friction coefficient at the contact patch	–
γ	Exponent of the power-law equation for soft hemicylindrical fingertips contacts	–
$\tilde{x}, \tilde{y}$	Nondimensionalized coordinates, $\tilde{x} = \frac{x}{l}, \tilde{y} = \frac{y}{a}$	–
$\Gamma()$	Gamma function	–

1. Introduction

Soft-finger contact mechanics plays an important role in both grasping stability and safe object prehension and handling during manipulation. When modeling contacts in robotic grasping and manipulation,[1] different types of nonlinear contacts have been proposed for analysis of soft finger (hemispherical soft fingertip,[1,2] cylindrical soft fingertip,[3] and hemicylindrical soft fingertip[4]). A general framework of "limit surface" is also progressing to possess a conceptual 3D surface within which the contact, with applicable contact interface accompanied by the applied forces and moments, will support without slip.[5–7] The limit surface became a very beneficial tool for modeling contact interface in robotic grasping and manipulation. Point contact with or without friction was first used to model contacts in robotics. The Coulomb friction law was used to model a point contact finger with friction. The friction limit surface in this state is a friction cone, with half of the conical included angle being $\theta = \tan^{-1}(\mu)$, where μ is the coefficient of friction at the contact interface.[8]

However, when the contact patch assumes finite area, the assumption of point contact is no longer applicable and needs to be extended to soft contact, which includes not only a friction (or traction) force at the contact interface but also a moment sustained due to the finite area of contact.[9,10] It has been shown that the limit surface of soft-finger contact resembles an ellipsoid with friction force and moment. As the materials and geometric design of fingertips diversify, as the materials the viscoelastic behavior of certain types of fingertips was noticed, the modeling of such contact finds applications in modeling of human and biomedical fingertips.[11]

From the literature review, it is clear that a substantial amount of work has been carried out on robots and robotic hands. Thus, many works have been carried out on the modeling of the mechanical contact force of anthropomorphic hemispherical and hemicylindrical soft fingertips. Also, there is no literature available to study the modeling of contact pressure profile and friction limit surface at contact zone for hemicylindrical soft fingers, where all literature assume the hemispherical contact for robotic finger. Therefore, in this study, the general characteristics of contact pressure profile at the contact zone for hemicylindrical soft fingers have been formulated; also, the limit surface in robotic grasping and manipulation has been developed.

2. Modeling of Contact Interface

Modeling of contact interface depends on the nature of bodies in contact including material properties, applied force, contact shape, deformation, and elastic properties.

2.1. Hertzian contact model

Elastic contact modeling was first studied and formulated more than a century ago by Hertz[12] in 1882 based on contact between two linear elastic materials with a normal force, which results in very small contact deformation. Timoshenko and Goodier[13,14] studied the contact between two parallel cylinders and found that analytically the intensity of pressure between the contacting surfaces could

https://doi.org/10.1017/S0263574713001215 Published online by Cambridge University Press

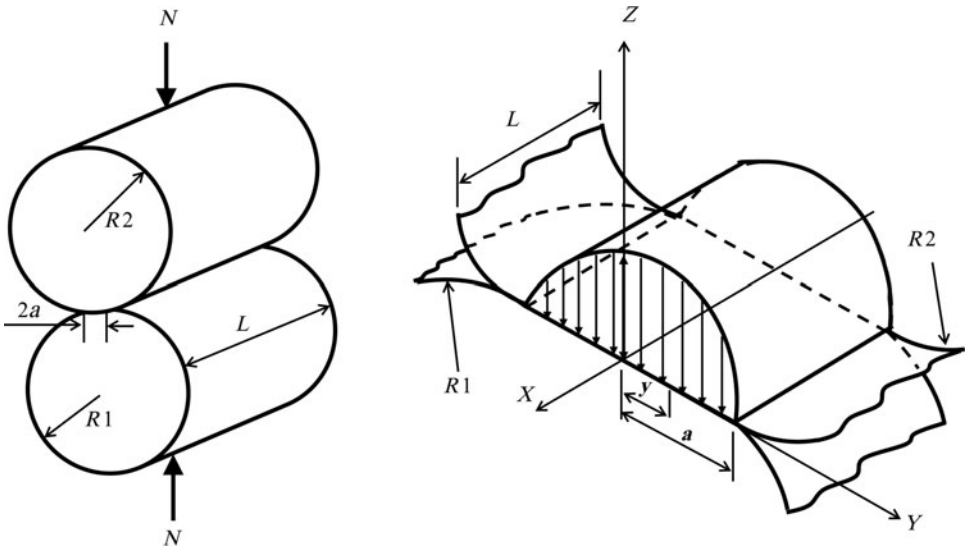

Fig. 1. (a) Contact of two parallel linear elastic cylinders; (b) pressure distribution for contacting parallel linear elastic cylinders 14.

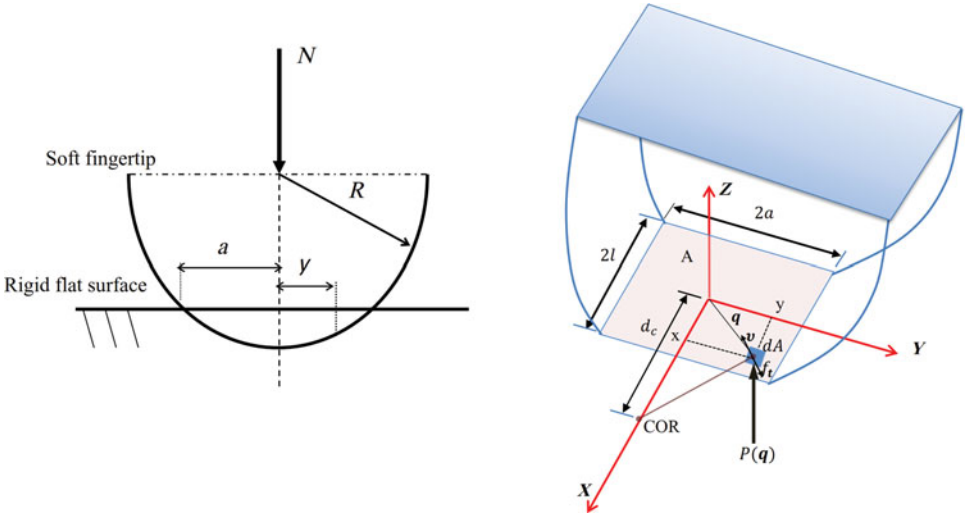

Fig. 2. (Colour online) (a) Geometry of contact between a hemicylindrical fingertip and a rigid surface; (b) contact and coordinates for COR and local infinitesimal area *dA* for numerical integration to construct the limit surface of soft fingers.

be represented by an elliptical (or, rather, semi-ellipsoid). For a symmetric and rectangular contact area, the pressure distribution is

$$p = \frac{2N}{\pi a L}\sqrt{1 - \left(\frac{y}{a}\right)^2}, \tag{1}$$

where N is the normal force, a is the half width contact of the rectangular contact area for hemicylindrical fingertips, L is the depth contact of the rectangular contact, and y is the distance from the center of contact, with $0 \leq y \leq a$, as shown in Fig. 1.[14]

2.2. *Contact model for soft finger*

A typical contact interface between a soft hemicylindrical fingertip and contact surface is illustrated in Fig. 2(a). In typical robotic contact interfaces, the materials of the fingertips are not linear elastic. A model that extends linear to nonlinear elastic contact was presented[4] with a power-law equation,

https://doi.org/10.1017/S0263574713001215 Published online by Cambridge University Press

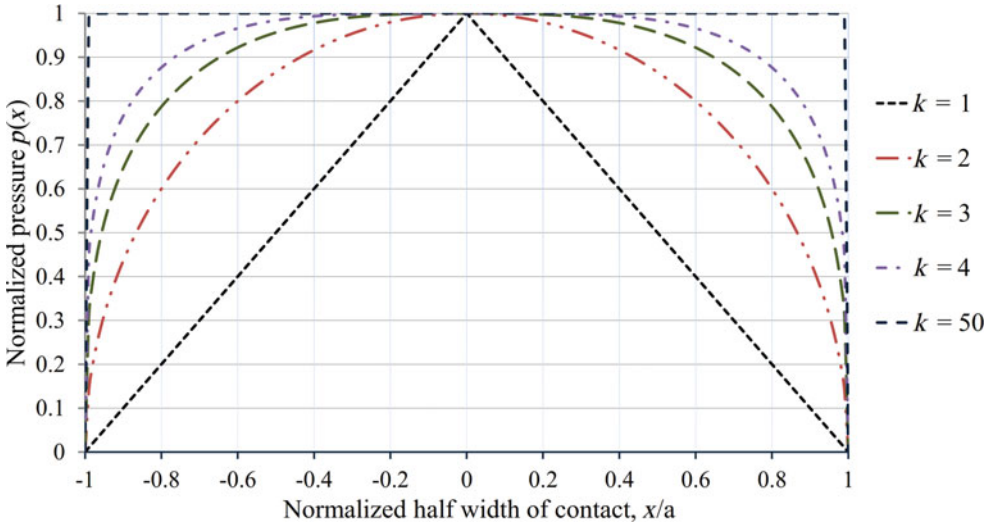

Fig. 3. (Colour online) Normalized pressure distribution for hemicylindrical fingertip with respect to the normalized axis, *y/a*. The plot shows an axisymmetric pressure distribution with $k = 1$, 2, 3, 4, and 50; the pressure profile becomes more like a uniformly distributed load.

which subsumes the Timoshenko and Goodier[13] contact theory,

$$a = c_{cy} N^{\gamma_{cy}}, \tag{2}$$

where $\gamma_{cy} = \frac{n}{n+1}$ is the exponent of the normal force that has range $0 \leq \gamma_{cy} \leq \frac{1}{2}$, N is the strain-hardening exponent, and c_{cy} is a constant depending on the size and curvature of the fingertip as well as the material properties.

2.3. Contact pressure distribution at soft finger

The Hertzian, Timoshenko, and Goodier[13] contact theory is considered. The assumed pressure distribution for small elastic deformation is given in Eq. (1). The pressure profile for two linear elastic cylinders in contact according to Timoshenko and Goodier[13] has ellipsoidal profile (or semi-ellipsoid). However, as the radius of curvature of the two asperities increases, and the material properties change to hyper-elastic, the pressure distribution becomes more uniform and eventually becomes almost square.[15,16] In the present study, a general pressure-distribution function that aims to capture material properties and contact geometry with various pressure profiles is introduced. Therefore, the pressure distribution for a rectangular contact area can be written in general form as follows:

$$p = C_k \frac{N}{\pi a L} \left(1 - \left(\frac{y}{a}\right)^k\right)^{\frac{1}{k}}, \tag{3}$$

where $\underline{k}$ determines the shape of the pressure profile, and C_k is a coefficient that adjusts for the profile of pressure distribution over the contact area to satisfy equilibrium condition. In Eq. (3), p is defined for $0 \leq y \leq a$. By symmetry, $p(y) = p(-y)$, when $-a \leq y \leq 0$. When k becomes larger, the pressure distribution approaches uniform distribution, as shown in Fig. 3. It is also required that the integral of the pressure over the contact area be equal to the normal force, that is,

$$\int_A p dA = \int_{-L/2}^{L/2} \int_{-a}^{a} p \mathrm{d}y \, \mathrm{d}x = N. \tag{4}$$

The coefficient C_k can be obtained by substituting Eq. (3) into Eq. (4). It is interesting to note that when Eq. (4) is integrated, both the normal force and the half width contact of the rectangular contact

https://doi.org/10.1017/S0263574713001215 Published online by Cambridge University Press

Table I. The coefficient of the pressure distribution for hemicylindrical fingertip.

k		C_k
1	Triangular	3.1416
2	Elliptical	2
3	Cubic	1.7782
4	Quadruple	1.6944
Infinity	Uniform	1.5708

area vanish, leaving only the constant C_k as follows:

$$C_k = \pi \frac{k\Gamma\left(\frac{2}{k}\right)}{\left[\Gamma\left(\frac{1}{k}\right)\right]^2}, \tag{5}$$

where $k = 1, 2, 3, \ldots$ and $\Gamma()$ is the Gamma function.[17] The numerical values of C_k for a few values of k are listed in Table I. A normalized pressure distribution with respect to the normalized axis, y/a, is plotted in Fig. 3. As can be seen from this figure, when k approaches infinity, the pressure profile will become that of a uniformly distributed load with magnitude of $N/(2aL)$, in which case $C_k = \frac{\pi}{2} = 1.5708$. Substituting values of the Gamma functions into Eq. (5), C_k can be found for any value of k as shown in Table I.

When $k = 1$, the pressure distribution is triangular with $C_k = \pi = 3.1416$. For linear elastic materials, $k = 2$ can be used, although it is found that $k \sim 1.8$ is also appropriate in some cases.[18] The general pressure-distribution function will be the same equation that was derived by Timoshenko and Goodier[13] (i.e., Eq. (1)). However, such pressure distribution is not very practical, especially in robotic grasping and manipulation. For nonlinear elastic and visco-elastic materials, the value of k tends to be higher, depending on the properties of the material. Combining Eqs. (3) and (5), the general pressure distribution becomes

$$p = \frac{N}{aL} \frac{k\Gamma\left(\frac{2}{k}\right)}{\left[\Gamma\left(\frac{1}{k}\right)\right]^2} \left(1 - \left(\frac{y}{a}\right)^k\right)^{\frac{1}{k}}. \tag{6}$$

3. Friction Limit Surface

Friction "limit surface" is a conceptual surface within which sliding does not occur; that is, the limit surface is the boundary between nonsliding and sliding motions in grasping and manipulation. The normal to the limit surface also is the instantaneous direction of sliding. Depending on contact types, friction limit surface takes different shapes.[1] A coordinate frame is defined so that the planar contact patch is in the $z = 0$ plane, and let $p(\boldsymbol{q}) \geq 0$ be the contact pressure distribution between the part and support as a function of the location $\boldsymbol{q}= (x, y)$. The friction coefficient at the contact patch is μ . If the planar velocity of the part is $\boldsymbol{u} = [\omega_z, v_x, v_y]^T$, then the linear velocity at $\boldsymbol{q}$ is

$$\boldsymbol{v}(\boldsymbol{q}) = (v_x - \omega_z y, v_y + \omega_z x)^T, \tag{7}$$

and the unit velocity is $\tilde{\boldsymbol{v}}(\boldsymbol{q}) = \boldsymbol{v}(\boldsymbol{q}) / \|\boldsymbol{v}(\boldsymbol{q})\|$. The infinitesimal force applied by the part to the support at q, in the plane of sliding, is

$$\mathrm{d}\boldsymbol{f}(\boldsymbol{q}) = [\mathrm{d}\boldsymbol{f}_x(q), \mathrm{d}\boldsymbol{f}_y(\boldsymbol{q})]^T = \mu p(q)\, \tilde{\boldsymbol{v}}(\boldsymbol{q}). \tag{8}$$

The total wrench the part applies to the support is

$$\boldsymbol{w} = \begin{pmatrix} m_z \\ f_x \\ f_y \end{pmatrix} = \int_A \begin{pmatrix} x\mathrm{d}f_{yx}(\boldsymbol{q}) - y\mathrm{d}f_y(\boldsymbol{q}) \\ \mathrm{d}f_x(\boldsymbol{q}) \\ \mathrm{d}f_y(\boldsymbol{q}) \end{pmatrix} dA. \tag{9}$$

https://doi.org/10.1017/S0263574713001215 Published online by Cambridge University Press

In this research, Fig. 2(b) shows a rectangular contact patch with an instantaneous center of rotation (COR). The following derivation is for the total friction force (f_t) and moment (m_z) on the rectangular contact interface for the COR at a distance dc along the X-axis. By varying the COR distance dc from $-\infty$ to ∞, all possible combinations of (f_t, m_z) can be found in order to construct the entire friction limit surface.[2,9] The tangential force over the entire contact area can be obtained by integrating shear force on each infinitesimal areas, dA, on which Coulomb's law of friction is observed, over the entire contact area A. When Timoshenko and Goodier[13] contact pressure distribution is considered, use $k = 2$ in Eq. (1). Setting $q = (x, y)^T$ and $q = q$, the total tangential force can be integrated using Eq. (8) to obtain

$$f_t = \begin{pmatrix} f_x \\ f_y \end{pmatrix} = -\int_A \mu \tilde{\boldsymbol{v}}(\boldsymbol{q})\, p(q)\, dA, \tag{10}$$

where $\boldsymbol{f}_t$ is the tangential force vector with the direction shown in Fig. 2(b), μ is the coefficient of friction, $\tilde{v}(\boldsymbol{q})$ is the unit vector in the direction of the velocity vector $v(q)$ with respect to the COR on the infinitesimal area dA at location q, and $p(q)$ is the pressure distribution at distance q from the center of contact. The minus sign denotes the opposite directions of $\tilde{v}(\boldsymbol{q})$ and $\boldsymbol{f}_t$. Since they are primarily interested in the magnitude of the friction force and moment, the sign will be omitted in the later derivation when magnitudes are concerned.

Similarly, the moment about the Z-axis, or the normal to the contact area, is

$$m_z = \int_A \mu \left\| \boldsymbol{q} \times \tilde{\boldsymbol{v}}(\boldsymbol{q}) \right\| p(q) \quad dA, \tag{11}$$

where $\|\boldsymbol{q} \times \tilde{v}(\boldsymbol{q})\|$ is the magnitude of the cross-product of the vectors $\boldsymbol{q}$ and $\tilde{v}(\boldsymbol{q})$, whose direction is normal to the contact surface.

The unit vector $\tilde{v}(\boldsymbol{q})$ is related to the distance d_c from the origin to the COR chosen on the X-axis from Fig. 2(b), and can be written as follows:

$$\tilde{v}(\boldsymbol{q}) = \frac{1}{\sqrt{(x - d_c)^2 + y^2}} \begin{bmatrix} -y \\ (x - d_c) \end{bmatrix}. \tag{12}$$

Due to symmetry, $f_x = 0$ for all CORs along the X-axis; therefore, the magnitude of the tangential force in the contact tangent plane is $f_t = f_y$. On substituting Eqs. (3) and (12) into Eqs. (10) and (11), we obtain

$$f_t = \int_A \mu \frac{(x - d_c)}{\sqrt{(x - d_c)^2 + y^2}} \frac{C_k N}{\pi a L} \left(1 - \left(\frac{y}{a}\right)^k\right)^{\frac{1}{k}} \quad dA. \tag{13}$$

Similarly, the moment about the Z-axis, or the normal to the contact area, is

$$m_z = \int_A \mu \frac{(x^2 - x d_c + y^2)}{\sqrt{(x - d_c)^2 + y^2}} \frac{C_k N}{\pi a L} \left(1 - \left(\frac{y}{a}\right)^k\right)^{\frac{1}{k}} \quad dA. \tag{14}$$

Equations (13) and (14) will be written in the simplest form (a normalized coordinate) so that they can be numerically integrated by using the following variables:

$$\tilde{x} = \frac{x}{l}, \quad \tilde{d}_c = \frac{d_c}{l}, \quad \tilde{y} = \frac{y}{a} \quad \text{and} \quad dA = dx \quad dy = al \quad d\tilde{y}\, d\tilde{x}, \tag{15}$$

where $l = \frac{L}{2}$ and the coefficient of friction μ is assumed constant throughout the contact area. Substituting the normalized coordinate Eq. (15) into Eq. (13) and dividing both sides by μN, one can

https://doi.org/10.1017/S0263574713001215 Published online by Cambridge University Press

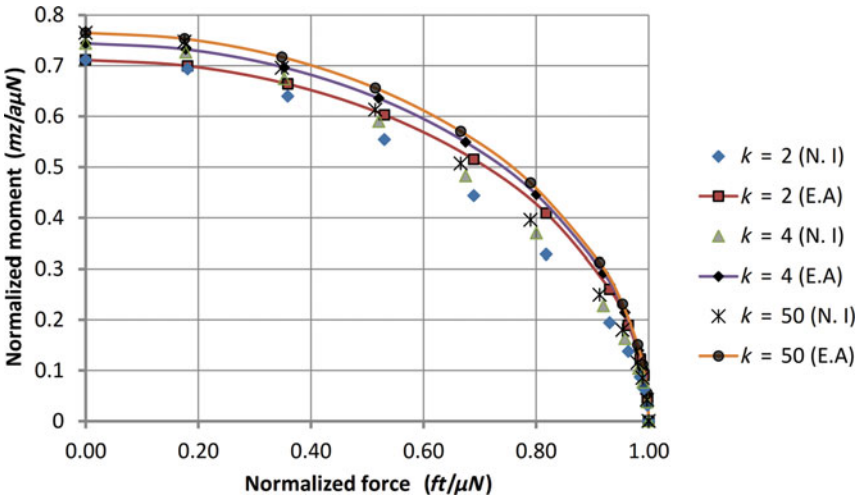

Fig. 4. (Colour online) Limit surface obtained by numerical integration (N.I) and elliptical approximation (E.A). The numerical integration is based on the pressure distribution, $p(q)$, and the coefficient, C_k. In this figure, the pressure distributions of $k = 2$, 4, and 50 are used.

derive

$$\frac{f_t}{\mu N} = \frac{C_k}{2\pi}\int_{-1}^{1}\int_{-1}^{1}\frac{(\tilde{x}-\tilde{d}_c)}{\sqrt{(\tilde{x}-\tilde{d}_c)^2+\left(\frac{\tilde{y}}{\beta}\right)^2}}(1-\tilde{y}^k)^{\frac{1}{k}}\,\mathrm{d}\tilde{y}\,\mathrm{d}\tilde{x}. \tag{16}$$

On substituting again Eq. (15) into Eq. (14) and dividing both sides by $a\mu N$, we obtain

$$\frac{m_z}{a\mu N} = \frac{C_k}{2\pi}\int_{-1}^{1}\int_{-1}^{1}\frac{(\beta^2\tilde{x}^2-\beta^2\tilde{x}\tilde{d}_c+\tilde{y}^2)}{\sqrt{\beta^2(\tilde{x}-\tilde{d}_c)^2+\tilde{y}^2}}(1-\tilde{y}^k)^{\frac{1}{k}}\,\mathrm{d}\tilde{y}\,\mathrm{d}\tilde{x}, \tag{17}$$

where $B = \frac{l}{a}$ is aspect ratio of rectangular contact, Eqs. (16) and (17) can be numerically integrated for different values of d_c or $\tilde{d}_c$ to yield a point on the limit surface for a prescribed pressure distribution $p(q)$ given by Eq. (3). Both equations involve elliptic integrals whose closed-form solutions may not exist but can be evaluated numerically. When the COR distance[2,6] dc varies from $-\infty$ to ∞, all possible combinations of $(\frac{f_t}{\mu N}, \frac{m_z}{a\mu N})$ can be obtained for plotting the friction limit surface.

4. Results and Discussions on the Limit Surface

Numerical integration for different values of (k) and $(\tilde{d}_c)$ yields pairs of $(\frac{f_t}{\mu N}, \frac{m_z}{a\mu N})$, as shown in Fig. 4. The normalized limit surface in Fig. 4 shows that as $dc \to \infty$, the normalized tangential force, $\frac{f_t}{\mu N}$, approaches its maximum value of 1, whereas the normalized moment, $\frac{m_z}{a\mu N}$, approaches zero. This corresponds to the case of pure translational sliding without rotation. On the other hand, as dc becomes 0, the normalized moment approaches its maximum values (0.7114 for $k = 2$, 0.7442 for $k = 4$, and 0.7649 for $k = 50$). The characteristic patch of a soft contact, very significant in the modeling of soft-finger and kinematic relationships,[19] is defined as the ratio between the maximum moment and maximum friction force, as shown in the limit surface of soft-finger; therefore, the normalized characteristic pitches of soft fingers based on the normalized limit surface are as follows:

$$\tilde{\lambda} = \frac{m_{z_{\max}}/a\mu N}{f_{t_{\max}}/\mu N} = \begin{array}{lll} 0.7114, & \text{when} & k = 2 \\ 0.7442, & \text{when} & k = 4 \\ 0.7649, & \text{when} & k = 50 \end{array}. \tag{18}$$

The characteristic pitch is defined as $\tilde{\lambda} = m_{z_{\max}}/f_{t_{\max}}$. An important result of Fig. 4 is that the contact pressure distribution affects the limit surface and the characteristic pitch. Values of characteristic pitch

https://doi.org/10.1017/S0263574713001215 Published online by Cambridge University Press

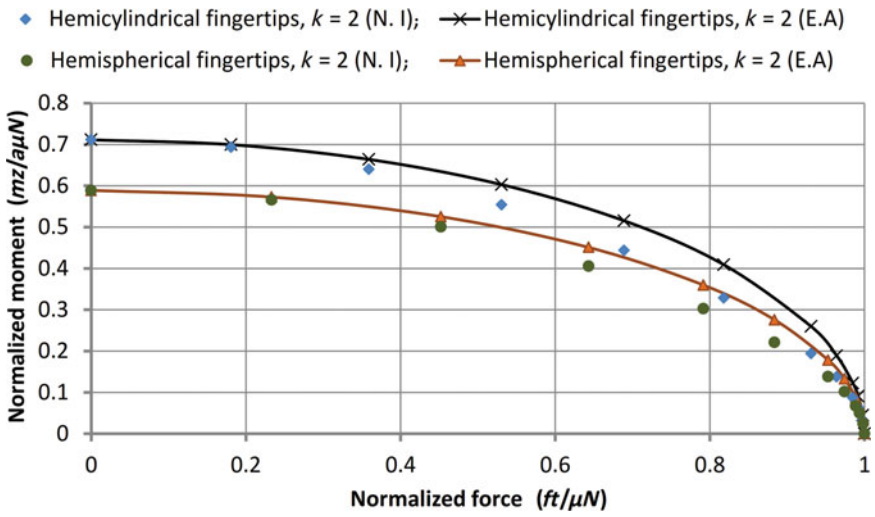

Fig. 5. (Colour online) The comparison of the friction limit surfaces of the hemicylindrical fingertips (present work) with those of the hemispherical fingertips,[2] obtained by numerical integration (N.I) and elliptical approximation (E.A). The numerical integration is based on the pressure distribution, $p(q)$, and the coefficient, C_k, from Table I. In this figure, the pressure distributions of $k = 2$ are used.

Table II. The normalized characteristic pitch.

	$\tilde{\lambda}$	
K	Hemispherical fingertip[2]	Hemicylindrical fingertip
2	0.589018	0.711375
4	0.63535	0.744213
50	0.6654	0.76494

can be obtained. Based on the results of the normalized limit surface, limit surfaces can be obtained by multiplying the normalized moment by $a\mu N$ and the normalized force by μN.

The results in Fig. 4 also suggest that the numerical integration yields a solution that is very close to the elliptical approximation. Without loss of generality, the friction-limit surface can be written in the form of

$$\left(\frac{f_t}{\mu N}\right)^2 + \left(\frac{m_z}{(m_z)_{\max}}\right)^2 = 1, \tag{19}$$

where the maximum moment $(m_z)_{\max}$is

$$(m_z)_{\max} = \int_A \mu \mid q \mid \frac{C_k N}{\pi a L}\left(1 - \left(\frac{x}{a}\right)^k\right)^{\frac{1}{k}} dA. \tag{20}$$

Obtained from Eq. (14) with the COR at $dc = 0$, this defines the quarter-elliptical curves in Fig. 4. For example, $(m_z)_{\max} = 0.7114\, a\mu N$ when $k = 2$. The half width contact of rectangular contact area a and the normal force N are related by Eq. (2), which depends on the soft-finger materials, normal force, contact size, and geometry.

The comparison of the friction limit surfaces of the hemicylindrical fingertips (present work) with those of the hemispherical fingertips,[2] as shown in Figs. 5–7 and Table II, with the same radius of fingertip, shape factor of the pressure profile, and applied load, shows that the zone of friction limit surfaces of the hemicylindrical fingertips is larger than the zone of friction limit surfaces of the hemispherical fingertips. More precisely, the friction limit surfaces are improved (13%–17%), as shown in Table III, if hemicylindrical fingertips are used rather than hemispherical fingertips in robot and robotic hand applications. The half width contact of the hemicylindrical fingertip can be

https://doi.org/10.1017/S0263574713001215 Published online by Cambridge University Press

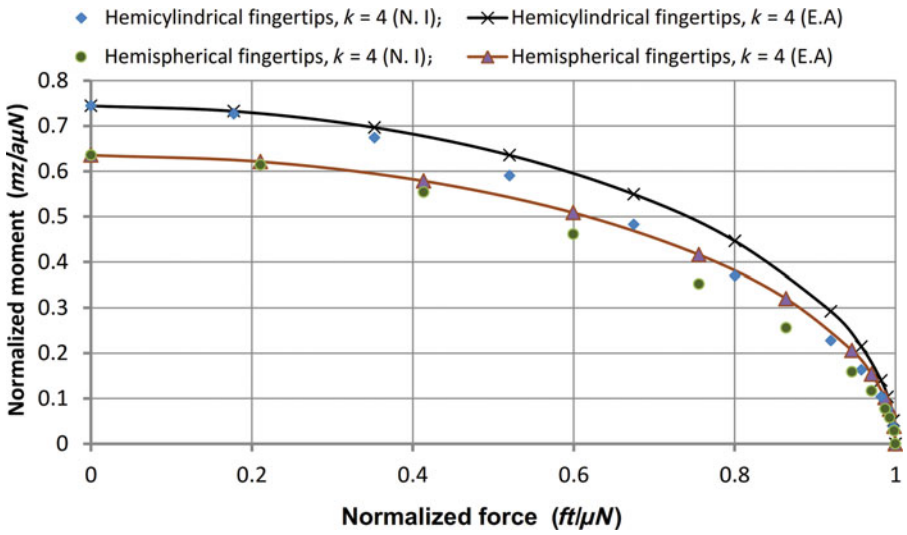

Fig. 6. (Colour online) The comparison of the friction limit surfaces of the hemicylindrical fingertips (present work) with those of the hemispherical fingertips,[2] obtained by numerical integration (N.I) and elliptical approximation (E.A). The numerical integration is based on the pressure distribution, $p(q)$, and the coefficient, C_k, from Table I. In this figure, the pressure distributions of $k = 4$ are used.

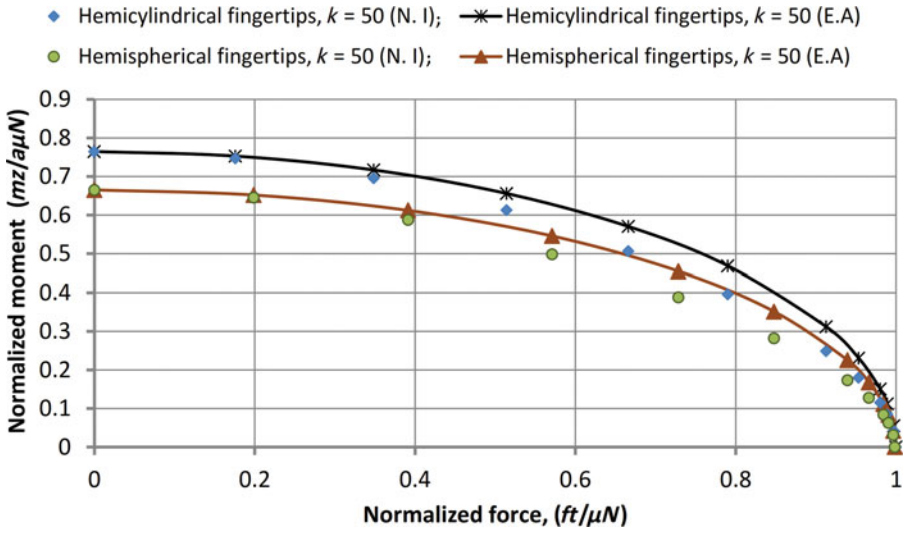

Fig. 7. (Colour online) The comparison of the friction limit surfaces of the hemicylindrical fingertips (present work) with those of the hemispherical fingertips,[2] obtained by numerical integration (N.I) and elliptical approximation (E.A). The numerical integration is based on the pressure distribution, $p(q)$, and the coefficient, C_k, from Table I. In this figure, the pressure distributions of $k = 2$ are used.

Table III. The comparison of friction limit surfaces between the hemicylindrical fingertips (present work) and hemispherical fingertips,[2] for different values of shape factor of the pressure distribution profiles ($k = 2, 4, 50$).

	Friction limit surface zone (nonsliding area)		
K	Hemispherical fingertip[2]	Hemicylindrical fingertip (present work)	Improvement (%)
2	0.4628	0.558938	17.2001
4	0.499204	0.584739	14.6279
50	0.522814	0.601024	13.0128

https://doi.org/10.1017/S0263574713001215 Published online by Cambridge University Press

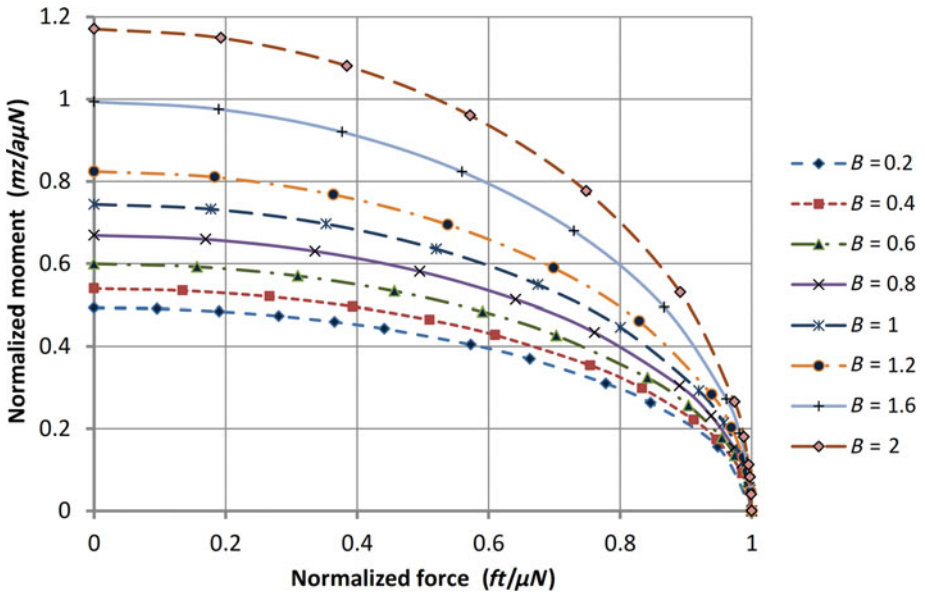

Fig. 8. (Colour online) The comparison of friction limit surfaces between the hemicylindrical fingertips (present work) obtained by numerical integration (N.I) at different values of the aspect ratio B. The numerical integration is based on the pressure distribution, $p(q)$, and the coefficient, C_k, from Table I. In this figure, the pressure distributions of $k = 4$ are used.

dominated easily, in the case of hemicylindrical fingertip, by altering the depth of the hemicylinder as shown in Fig. 8, while this is limited in the case of hemispherical tip due to axis symmetry. As illustrated in Fig. 8, the limit surface reduces inward with respect to the unit normalized force, $\frac{f_t}{\mu N}$, as the aspect ratio of rectangular contact B decreases, by assuming that the pressure distribution, and thus C_k, do not change. In addition, it was found that hemicylindrical shape fingertips are desired for the applications of robotic hands and prosthetic hands.

5. Conclusions

In this study, it is shown that the general pressure-distribution function in Eq. (3) can be used for linear elastic contact as well as soft (nonlinear elastic) contact. If the contact is harder and behaves more like linear elastic materials, the coefficient of pressure distribution over the contact area will be equal to 2, reflecting the linear elastic model predicted by Timoshenko and Goodier.[13] Furthermore, the coefficient of pressure distribution over the contact area is found between π and $\pi/2$.

The normalized limit surface for a soft finger can be calculated by numerical integration with a known pressure distribution. The numerical results are close to the elliptical approximation. In addition, the normalized characteristic pitch is found, the ratio between the maximum normalized moment and force is $\tilde{\lambda} = 0.7114$ for the second-order pressure distribution at the contact, $\tilde{\lambda} = 0.7442$ for the fourth-order pressure distribution, and $\tilde{\lambda} = 0.7649$ for the uniform pressure distribution. It is found that friction limit surfaces are ameliorated if hemicylindrical fingertips are used rather than hemispherical fingertips. So, the friction limit surfaces of hemicylindrical shape fingertips are required over hemispherical shape fingertips for robotic hand and prosthetic hand applications. The combination of the friction-limit surface and the soft finger contact-mechanics model will help to analyze and simulate contact behaviors of grasping and manipulation in robotics that involve contacts with soft fingers.

Acknowledgements

The author would like to acknowledge Prof. Rolf Pfeifer and Dr. Alejandro Hernandez Arieta, Artificial Intelligence Laboratory, University of Zurich, Switzerland for their help and assistance. Thanks are also due to the Ministry of Higher Education and Scientific Research, Iraq.

References

1. I. Kao, K. Lynch and J. W. Burdick, "Contact modeling and manipulation," **In**: *Springer Handbook of Robotics* (B. Siciliano and O. Khatib, eds.) (Springer, Berlin, 2008) pp. 647–669.
2. N. Xydas and I. Kao, "Modeling of contact mechanics and friction limit surface for soft fingers in robotics, with experimental results," *Int. J. Robot. Res.* **18**(8), 941–950 (1999).
3. N. Elango and R. Marappan, "Development of contact model of a robot soft finger for power grasping and determination of its contact width," *Int. J. Recent Trends Eng.* **1**(5), 5–9 (2009).
4. S. H. Bakhy, S. S. Hassan, S. M. Nacy, K. Dermitzakis and A. H. Arieta, "Contact mechanics for soft robotic fingers: Modeling and experimentation," *Robotica* **31**(4), 599–609 (2013).
5. S. Goyal, A. Ruina and J. Papadopoulos, "Planar sliding with dry friction: Part 1. Limit surface and moment function, and Part 2. Dynamics of motion," *Wear* **143**, 307–352 (1991).
6. R. D. Howe and M. R. Cutkosky, "Practical force-motion models for sliding manipulation," *Int. J. Robot. Res.* **15**(6), 555–572 (1996).
7. N. Xydas and I. Kao, "Modeling of Contacts and Force/Moment for Anthropomorphic Soft Fingers," *Proceedings of the International Conference on Intelligent Robots and Systems (IROS)*, Victoria, Canada (1998) pp. 488–493.
8. Y. Li and I. Kao, "A Review of Modeling of Soft-Contact Fingers and Stiffness Control for Dexterous Manipulation in Robotics," *Proceedings of the IEEE International Conference on Robotics and Automation (ICRA)*, Seoul, South Korea (2001) pp. 3055–3060.
9. R. D. Howe, I. Kao and M. R. Cutkosky, "Sliding of Robotic Fingers Under Combined Torsion and Shear Loading," *Proceedings of the International Conference on Robotics and Automation (ICRA)*, Philadelphia, USA (1988) pp. 103–105.
10. K. B. Shimoga and A. A. Goldenberg, "Soft robotic fingertips – Parts I and II: A comparison of construction materials," *Int. J. Robot. Res.* **15**(4), 320–334 (1996).
11. C.-H. Dylan Tsai, I. Kao, M. Higashimori and M. Kaneko, "Modeling, sensing, and interpretation of viscoelastic contact interface," *Adv. Robot.* **26**(11–12), 1393–1418 (2012).
12. H. Hertz, "On the contact of elastic solids," *J. Reine Angew. Math.* **92**, 156–171 (1881).
13. S. P. Timoshenko and J. N. Goodier, *Theory of Elasticity*, 3rd ed. (McGraw-Hill, Tokyo, 1970) pp. 414–420.
14. E. J. Hearn, *Mechanics of Materials Part (2): Introduction to the Mechanics of Elastic and Plastic Deformation of Solids and Structural Materials*, 3rd ed. (Antony Rowe, Eastbourne, UK, 2001) pp. 386–387.
15. W. Emil, *Progress in Optics*, Vol. 30 (North-Holland, New York, 1992).
16. E. J. Nicolson and R. S. Fearing, "The Reliability of Curvature Estimates from Linear Elastic Tactile Sensors," *Proceedings of the IEEE International Conference on Robotics and Automation*, Washington, DC, USA (1995), Vol. 1, pp. 1126–1133.
17. E. Kreyszig, *Advanced Engineering Mathematics*, 9th ed. (John Wiley, New York, 2006) pp. 192–193.
18. S.-F. Chen Kao, Y. Li and G. Wang, "Application of bio-engineering contact interface and MEMS in robotic and human augmented systems," *IEEE Robot. Autom. Mag.* **10**(1), 47–53 (2003).
19. I. Kao, X. Wu and S. Chen, "Dual relationship in dexterous sliding manipulation under force and position control," *Int. J. Robot. Autom.* **14**(2), 68–77 (1999).